Title

Soft x-ray spectroscopy of high pressure liquid

Journal

Review of Scientific Instruments, 89(1)

ISSN

0034-6748

Authors

Qiao, Ruimin

Xia, Yujian

Feng, Xuefei

et al.

Publication Date

2018

DOI

10.1063/1.5008444

Peer reviewed

Soft x-ray spectroscopy of high pressure liquid

Ruimin Qiao, Yujian Xia, Xuefei Feng, James Macdougall, John Pepper, Kevin Armitage, Jason Borsos, Kevin G. Knauss, Namhey Lee, Arnaud Allézy, Benjamin Gilbert, Alastair A. MacDowell, Yi-Sheng Liu, Per-Anders Glans, Xuhui Sun, Weilun Chao, and Jinghua Guo

Citation: Review of Scientific Instruments **89**, 013114 (2018); doi: 10.1063/1.5008444

View online: https://doi.org/10.1063/1.5008444

View Table of Contents: http://aip.scitation.org/toc/rsi/89/1

Published by the American Institute of Physics

Soft x-ray spectroscopy of high pressure liquid

Ruimin Qiao,[1,a)] Yujian Xia,[1,2,a)] Xuefei Feng,[1] James Macdougall,[3] John Pepper,[1] Kevin Armitage,[1] Jason Borsos,[1] Kevin G. Knauss,[4] Namhey Lee,[4] Arnaud Allézy,[5] Benjamin Gilbert,[4] Alastair A. MacDowell,[1] Yi-Sheng Liu,[1] Per-Anders Glans,[1] Xuhui Sun,[2] Weilun Chao,[3,b)] and Jinghua Guo[1,b)]

[1]*Advanced Light Source, Lawrence Berkeley National Laboratory, 1 Cyclotron Road, Berkeley, California 94720, USA*

[2]*Jiangsu Key Laboratory for Carbon-Based Functional Materials & Devices, Institute of Functional Nano & Soft Materials (FUNSOM), Joint International Research Laboratory of Carbon-Based Functional Materials and Devices, Soochow University, Suzhou 215123, Jiangsu, China*

[3]*Center for X-Ray Optic, Lawrence Berkeley National Laboratory, Berkeley, California 94720, USA*

[4]*Energy Geoscience Division, Lawrence Berkeley National Laboratory, Berkeley, California 94720, USA*

[5]*Engineering Division, Lawrence Berkeley National Laboratory, Berkeley, California 94720, USA*

(Received 6 October 2017; accepted 5 January 2018; published online 30 January 2018)

We describe a new experimental technique that allows for soft x-ray spectroscopy studies (~100-1000 eV) of high pressure liquid (~100 bars). We achieve this through a liquid cell with a 100 nm-thick Si_3N_4 membrane window, which is sandwiched by two identical O-rings for vacuum sealing. The thin Si_3N_4 membrane allows soft x-rays to penetrate, while separating the high-pressure liquid under investigation from the vacuum required for soft x-ray transmission and detection. The burst pressure of the Si_3N_4 membrane increases with decreasing size and more specifically is inversely proportional to the side length of the square window. It also increases proportionally with the membrane thickness. Pressures > 60 bars could be achieved for 100 nm-thick square Si_3N_4 windows that are smaller than 65 μm. However, above a certain pressure, the failure of the Si wafer becomes the limiting factor. The failure pressure of the Si wafer is sensitive to the wafer thickness. Moreover, the deformation of the Si_3N_4 membrane is quantified using vertical scanning interferometry. As an example of the performance of the high-pressure liquid cell optimized for total-fluorescence detected soft x-ray absorption spectroscopy (sXAS), the sXAS spectra at the Ca *L* edge (~350 eV) of a $CaCl_2$ aqueous solution are collected under different pressures up to 41 bars. *Published by AIP Publishing.*
https://doi.org/10.1063/1.5008444

I. INTRODUCTION

Modern scientific research always relies on the development of advanced characterization techniques, which has greatly expanded the horizon of our knowledge. Techniques such as x-ray spectroscopy utilize interactions between x-rays and the core electrons of matter to provide fundamental information related to the local geometry and/or electronic structure of the sample with element sensitivity. In particular, soft x-ray absorption spectroscopy (sXAS) with the incident photon energy below 1 keV can reach critical core electron levels, such as C, N, and O *K*-edge as well as transition metal (TM) *L*-edge, which allows for the direct probing of the chemically important C, N, O 2*p* and TM 3*d* valence electron states through electric dipole allowed transitions.[1] Moreover, both surface and bulk sensitive information can be obtained simultaneously through the different detection channels of sXAS. Over the past several decades of development, sXAS has become a well-established technique that finds its applications in many different scientific fields, including molecular and condensed matter physics,[2–4] material science and engineering,[5,6] chemistry,[7–10] and biology and earth science.[11,12]

The sXAS technique has been widely adopted for studying solid samples of different forms; however, its application to gaseous samples, solutions, solid/gas, and solid/liquid interfaces is rather challenging as these systems are not compatible with the vacuum environment required by sXAS measurement due to the strong interaction of soft x-rays with the atmosphere. Different approaches have been developed in order to overcome this incompatibility, and these include differential pumping, liquid jet combined with a cryotrap, and a variety of liquid and gas cells.[13–26] The differential pumping technique helps us to create a relatively high vapor pressure space (~100 mbars) around the sample, while keeping the rest of the instrumental volume under adequate vacuum required for soft x-ray and electron transportation. In the case of liquids, a micro-jet nozzle is used to inject liquid directly into the differentially pumped analysis chamber, and the liquid sample is collected using a cryotrap. However, equilibrium conditions, well-controlled pressure and temperature are difficult to achieve with such setups. To allow better control, various liquid and gas cells have been developed, in which the liquid or gas is separated from the vacuum by a thin membrane window. Due to the low transmittance of soft x-ray, the membrane has to be composed of light elements, such as beryllium (Be), silicon nitride (Si_3N_4), and polyimide (PI), with the thickness normally less than a few hundred nanometers. The fabrication of Si_3N_4 membrane

a)R. Qiao and Y. Xia contributed equally to this work.
b)Authors to whom correspondence should be addressed: wlchao@lbl.gov and jguo@lbl.gov.

windows utilizes well-established silicon microfabrication techniques, with which heating/ cooling, electric bias, and other functions could also be easily integrated into the same chip. As a result, the reliability and versatility of the Si_3N_4 window have opened unprecedented opportunities for the studies of materials and reactions in practical conditions. Over the past a few years, Si_3N_4 window based gas/liquid cells equipped with multiple functions, such as high temperature reaction[18,20] and *in situ* electrochemical reaction,[14,17] have been developed.

However, due to the delicate nature of the thin Si_3N_4 membrane, these experiments have only been done at or slightly above ambient pressure to date. In fact, many technological and environmentally important processes occur at elevated temperature and pressure. For example, the Earth's lithostatic pressure gradient is ~220 bars/km, and the thermal gradient is ~25 °C/km; so studies relevant to subsurface fluids, including hydrothermal aqueous fluids and hydrocarbons and mineral surfaces, require pressure-compatible apparatus.[27] Soft-X-ray spectroscopy could provide insights into chemical reactions associated with ore formation,[28] shale reservoir and caprock evolution,[12] and geothermal systems.[29] In addition, the ability to study subcritical and supercritical carbon dioxide (critical temperature at 31.1 °C and critical pressure at 73.9 bars) will be of great utility for the application of this fluid as a green synthesis medium,[30] the development of photoelectrochemical mechanisms of CO_2 reduction,[31] and improved prediction of the chemical processes involved for successful subsurface geological carbon sequestration.[32]

In this paper, we carry out comprehensive studies on the burst pressure and deformation of the Si_3N_4 window for soft x-ray spectroscopy applications in high pressure liquids. The effects of changing size and thickness of the Si_3N_4 membrane as well as the thickness of the Si wafer are investigated. The high pressure liquid cell optimized for detecting soft x-ray absorption spectroscopy in total fluorescence yield mode is presented. We also demonstrate the first soft x-ray absorption spectra collected under different pressures up to 41 bars at the Ca *L*-edge (~350 eV) of a $CaCl_2$ aqueous solution.

II. Si_3N_4 MEMBRANE WINDOWS AND THE HIGH PRESSURE SOFT X-RAY CELL

The fabrication of the Si_3N_4 membrane window takes advantage of the anisotropic etching of the (100) oriented single crystal silicon as well as the smoothness and rigidity of the thin self-supporting Si_3N_4 film.[33,34] The anisotropic etching rate of silicon in a strong alkaline solution decreases in the order (100), (110), and (111). Figure 1(a) shows the front view of the Si_3N_4 membrane window. The cavity formed by etching is truncated pyramidal in shape, bounded by four sidewalls which represent the slowest etching (111) crystal planes forming an angle of 54.7° with the (100) surface plane. The fabrication was done at the Center for X-Ray Optics (CXRO) in Lawrence Berkeley National Lab (LBNL). Si (100) wafers coated with thin Si_3N_4 films on both sides were purchased from Addison Engineering, Inc. The Si_3N_4 coating on one side of

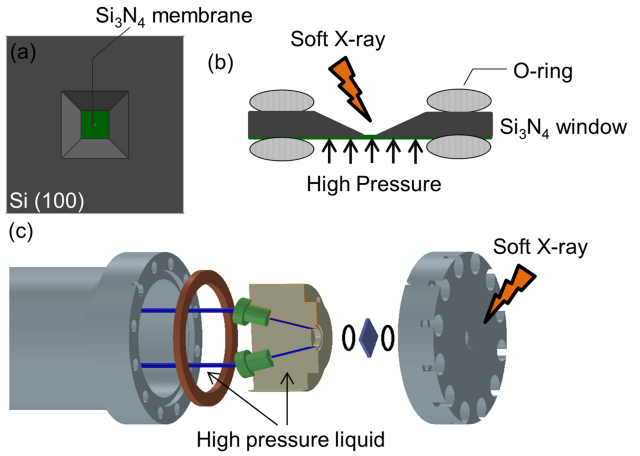

FIG. 1. Si_3N_4 membrane window and the high-pressure soft x-ray cell. (a) Front view of the Si_3N_4 window. (b) A diagram showing the principle of the high-pressure cell. (c) The assembly drawing of the high-pressure soft x-ray cell.

the wafer becomes the transparent membrane window through a process of optical lithography, which removes a specific pattern of Si_3N_4 on the opposing side as well as a similar pattern of the Si bulk material between them. A spin-coating process applies a UV sensitive photoresist to one side of the wafer onto which is transferred the array pattern of individual windows. In addition, the pattern includes cleaving lines, which specify the individual Si frames surrounding each window. The window pattern with cleave lines is imaged to the photoresist by UV exposure through pre-engineered Cr on a glass photomask which is carefully aligned to the Si crystal lattice by use of a mask aligner. A bath of developer removes the photoresist exposed through the mask leaving the unexposed resist intact. Thus, the window pattern with cleave lines is defined by the imaged side Si_3N_4 coating in a field of photoresist. The imaged side of the wafer is then subjected to a reactive ion etch which removes all the exposed Si_3N_4 leaving the unexposed Si_3N_4 under the resist intact. After removing the remaining resist, the imaged side of the wafer shows the window and frame lines pattern of exposed Si bulk in a field of the remaining Si_3N_4 coating. A bath in a 30% solution of potassium hydroxide at 80 °C preferentially etches the exposed Si bulk material all the way through the wafer thickness to the unexposed side of the wafer leaving the Si_3N_4 coated areas on both sides of the wafer intact. The cleave lines have been specifically configured to limit the depth of the lines to typically 40% of the wafer thickness. The designed pattern of Si_3N_4 membrane windows then exists on the unexposed side of the wafer, and a pattern of cleaving lines defining the individual window frames exist on the exposed side along with the pattern of etched divots, which create the window openings through the wafer.

For our study of the application of the Si_3N_4 membrane window for high-pressure sXAS, a series of different windows were fabricated. The study focuses on the size and thickness dependence of the burst pressure of the Si_3N_4 membrane. The impact of other factors, such as Si frame thickness, is also investigated. The baseline of the study is the burst pressure of

the square Si_3N_4 windows with 100 nm thick Si_3N_4 membrane and 500 μm thick Si frame, as a function of the membrane size, which is varied in the range of 5 μm–1 mm. The effects of varied Si_3N_4 membrane thickness (100 nm, 200 nm, and 500 nm) and Si frame thickness (200 μm and 500 μm) are also studied. Unless otherwise mentioned, the Si_3N_4 membrane is in low tensile stress (<250 MPa ± 50 MPa), and the dimension of the Si frame is 6.35 mm × 6.35 mm.

Figure 1(b) shows the principle of the high pressure sXAS cell. It utilizes two identical Viton O-rings with the outer diameter (OD) of 6 mm and inner diameter (ID) of 4 mm to support the Si_3N_4 window. The bottom O-ring also has the function to confine the high-pressure liquid, while the top O-ring seals the vacuum from the atmosphere in the case of sXAS experiments. Figure 1(c) shows the assembly drawing of the high pressure sXAS cell. The cap is made of stainless steel with a center conical hole to reveal the Si_3N_4 membrane window. The holder has one inlet and one outlet to allow liquid to flow, and it is made of polyether ether ketone (PEEK) allowing for electrical isolation which would accommodate later developments requiring electrical contacts relevant for *in situ* electrochemical experiments using sXAS. The liquid volume of the cell is about 1.5 mm^3. The high-pressure liquid is applied on the flat side of the Si_3N_4 window using a Teledyne Isco 100DM syringe pump operating in constant pressure mode. The three-dimensional (3D) deformation of the Si_3N_4 window in response to the applied hydrostatic pressure is quantified using vertical scanning interferometry (Zygo NewView™ 7300 with a 50× Mirau objective). All the burst pressure and deformation testing is carried out at 1 bar ambient pressure. For high pressure sXAS experiments, the stainless steel cap is affixed to a long tube with flange, which allows it to be positioned in the high vacuum analysis chamber [Fig. 1(c)]. The sXAS measurements are performed at the undulator beamline, BL 8.0.1 of Advanced Light Source (ALS),[35] in LBNL.

III. BURST PRESSURE AND DEFORMATION TESTING

The size dependence of the burst pressure of the Si_3N_4 membrane window is plotted in Fig. 2 in the log-log scale. It is evident that the data can be divided into two regions. Below 60 bars, burst pressure is inversely proportional to the side length of the square Si_3N_4 membrane window. The one-to-one correspondence between membrane size and burst pressure in this range is also listed at the right-hand side of Fig. 2. However, when the burst pressure goes above 60 bars, a strong deviation from the linear line is observed. In this region, the burst pressure only shows weak size dependence, and the variation of the burst pressure data increases as the membrane size reduces. We noticed that when the burst pressure is below 60 bars, the Si_3N_4 membrane bursts while the Si frame stays intact. In sharp contrast, the Si frame always breaks if the burst pressure is above 60 bars. This suggests that the tested burst pressure above 60 bars is actually the breaking pressure of the Si frame in the current supporting structure (Fig. 1). The observations clearly show that above 60 bars, the breaking of the single crystal Si frame has become the limiting factor. In a later section, we will discuss more about the factors related to the breaking of the Si frame.

The data demonstrate the utility of Si_3N_4 membranes for high-pressure studies. The burst pressure of the 1 mm Si_3N_4 membrane window is about 3 bars, which is already good for an ambient pressure sXAS experiment. For high pressure sXAS, it is shown that a 65 μm Si_3N_4 window can stand the impressively high pressure up to 59 bars. In fact, if the Si frame does not break, a 5 μm large and 100 nm thick Si_3N_4 membrane should be able to stand a pressure of 795 bars as regression predicts. Because modern soft X-ray beamlines can achieve a small focused beam size at the sample (e.g., the beam spot of the Beamline 8.0.1 at ALS can be focused down to 25 μm on the sample[35]), small Si_3N_4 membrane windows can be used and will not be an issue for the high pressure sXAS experiment.

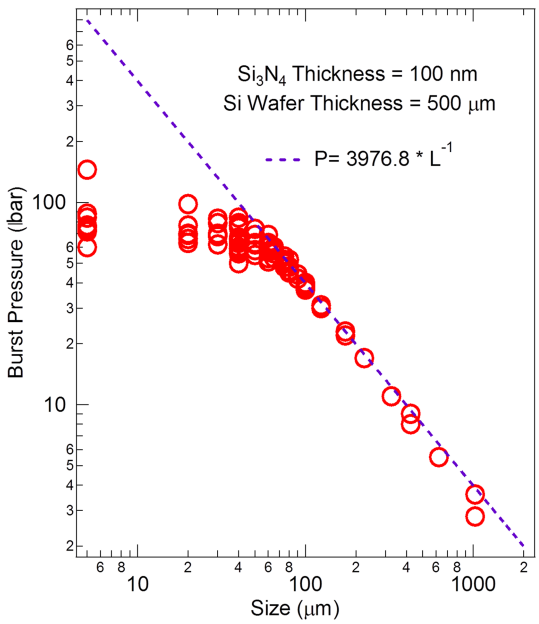

Size (μm)	Burst Pressure (bar)
1027	3
624	5.5
424	8.5
325	11
224	17
173	22.5
124	30.5
100	38.5
90	43
80	47
75	51
65	59

FIG. 2. Size dependence of the burst pressure of the Si_3N_4 membrane window in a log-log plot. The Si_3N_4 membrane thickness is 100 nm, and the Si frame thickness is 500 μm. Other specifications include low tensile stress Si_3N_4 membrane < 250 MPa ± 50 MPa, Si frame dimension = 6.35 mm × 6.35 mm.

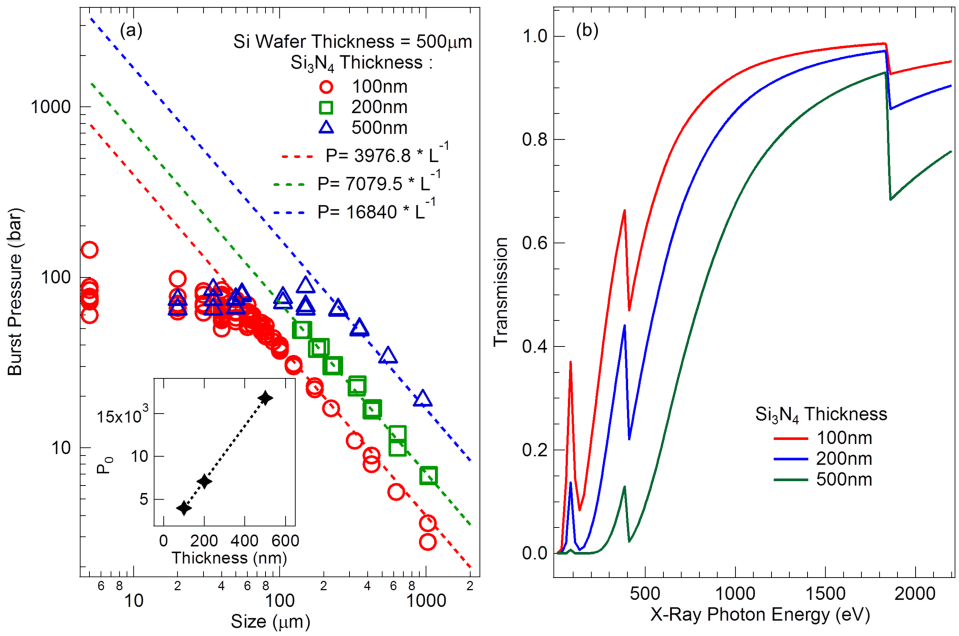

FIG. 3. (a) Burst pressure of the Si_3N_4 windows with different membrane thicknesses plotted as a function of the membrane size in a log-log scale. The membrane thickness dependent coefficient P_0 (from $P = P_0\ L^{-1}$) is plotted in the inset figure. The Si frame thickness is 500 μm. Other specifications include low tensile stress Si_3N_4 membrane < 250 MPa $\pm$ 50 MPa, Si frame dimension = 6.35 mm $\times$ 6.35 mm. (b) X-ray transmittance through the Si_3N_4 membrane of different thickness as a function of the photon energy.

Besides membrane size, membrane thickness is another important factor that affects the burst pressure of the Si_3N_4 window. In Fig. 3(a), we plot the burst pressure of the Si_3N_4 windows of different membrane thicknesses (100 nm, 200 nm, and 500 nm), as a function of the membrane size. The burst pressure is inversely proportional to the membrane size below 60 bars regardless of the membrane thickness. Above 60 bars, the Si frame starts to break and the tested burst pressure is that of the Si frame breaking pressure. As the thickness of the Si_3N_4 membrane is three orders of magnitude thinner than the Si frame (500 μm), the impact of the different Si_3N_4 membrane thicknesses on the Si frame breaking pressure is negligible. Moreover, based on the burst pressure data below 60 bars, we can deduce the membrane thickness dependent coefficient P_0, which is from $P = P_0\ L^{-1}$ [P is the burst pressure (bar) and L is the size (μm)]. The relation between P_0 and membrane thickness is plotted in the inset of Fig. 3(a), showing that the burst pressure of the Si_3N_4 window is inversely proportional to the membrane thickness.

Although a thicker Si_3N_4 membrane window holds higher pressure, its application in sXAS is limited by the low transmittance. Figure 3(b) shows the transmittance of soft x-ray in the photon energy range of 1–2200 eV through the Si_3N_4 membrane of different thicknesses. The x-ray transmittance follows an overall logarithmic growth with respect to the photon energy, except for the three sudden drops due to the absorption of Si_3N_4 at Si *L*-edge (~135 eV), N *K*-edge (~410 eV), and Si *K*-edge (~1860 eV). Meanwhile, the difference among the transmittance of the different Si_3N_4 membrane thicknesses is larger at lower photon energy, which gradually decreases for the higher photon energy. For example, the transmittance at C *K*-edge (~285 eV) is 46% for 100 nm-thick Si_3N_4, 21% for 200 nm, and only 2% for 500 nm. Therefore, 500 nm-thick Si_3N_4 will most likely not be suitable for C *K*-edge sXAS measurement. At O *K*-edge (~545 eV), the transmittance becomes 68% (100 nm), 46% (200 nm), and 15% (500 nm), and at Fe *L*-edge (~710 eV) it further increases to 82%, 68%, and 38%, respectively. For sXAS measurements in this range, a trade-off can be made by considering the desired pressure, available beam size, and transmittance for different Si_3N_4 window thicknesses. At the photon energy of 1000 eV, the transmittance reaches 92%, 85%, and 68% corresponding to the Si_3N_4 thickness of 100 nm, 200 nm, and 500 nm, respectively. The Si_3N_4 thickness has less impact on the x-ray transmittance when the photon energy is above 1000 eV.

As stated above, the Si frame of the Si_3N_4 membrane window starts to break above a certain pressure, which becomes the limitation of the high pressure sXAS application. In order to study factors related to the Si frame breaking, we compare the burst pressure curves of Si_3N_4 membrane windows of different Si frame thicknesses, 500 μm and 200 μm, as shown in Fig. 4. For the two sets of data, all the parameters except for the Si frame thickness are the same, including the same Si_3N_4 membrane specification and the same testing setup. The thickness of the Si_3N_4 membrane is 100 nm. At low pressure, they both follow the same linear path in the log-log plot because the burst pressure is inversely proportional to the Si_3N_4 membrane size. For Si_3N_4 windows with 200 μm thick Si frames, the divergence from this linear line due to wafer breaking happens at around 10 bars, which is far less than 60 bars for those with a 500 μm thick Si frame. The results clearly demonstrate that Si_3N_4 membrane bursting and Si frame breaking are two independent factors that affect the burst pressure of the Si_3N_4 window. Although a thicker Si frame is more resilient to the high pressure, we would like to point out for the same sized Si_3N_4 window, a thicker Si frame creates bigger opening on the front side of the window [Fig. 1(a)] due to the anisotropic etching, which in turn reduces the frame strength. Therefore, it might not be feasible to keep increasing the frame thickness in order to raise its breaking pressure. Other than the thickness of the Si frame, we believe that the defects (such as pin holes)

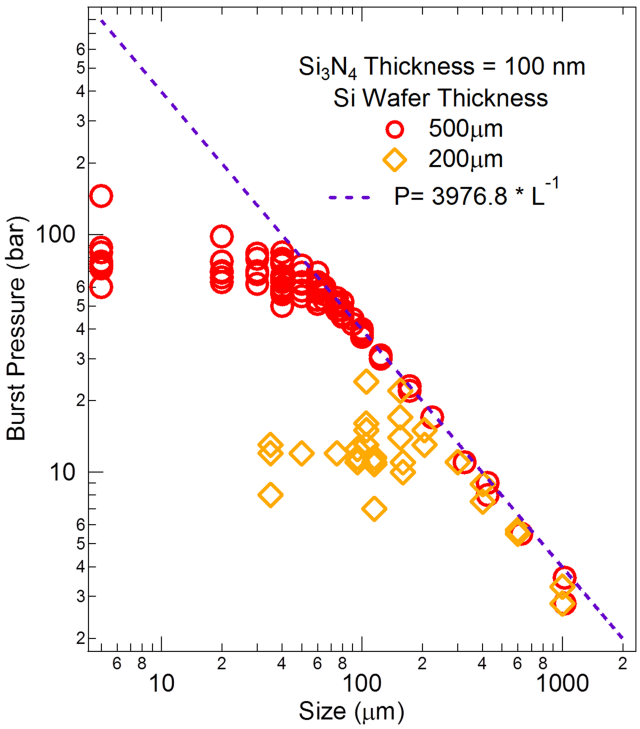

FIG. 4. Size dependence of the burst pressure of the Si_3N_4 window with different Si frame thicknesses in a log-log plot. The dimension of the Si frame is 6.35 mm × 6.35 mm × 500 (or 200) μm. The Si_3N_4 membrane is 100 nm thick and in low tensile stress (<250 MPa ± 50 MPa).

of the Si_3N_4 film also play an important role because these defects would not only compromise the membrane strength but also allow holes to be formed on the frame surface during the KOH etch, reducing the frame strength. This could explain the variation observed on the wafer breaking pressure (from 60 bars to 150 bars for 500 μm thick Si frames). Moreover, the choice of O-rings could also affect the deformation of the Si frame. Here, we choose two identical O-rings to support the Si wafer as one of the optimized conditions. In addition, the wafer breaking issue could be mitigated by restraining its deflection under high pressure through methods such as reducing the area under high pressure fluid and/or designing a better supporting structure for the Si frame. These approaches are currently under development.

In order to delve deeper into the mechanical properties of the thin Si_3N_4 membrane, the deformation of the membrane under increased pressures is quantified using vertical scanning interferometry (Zygo NewView 7300 with a 50× Mirau objective). The dimension of the tested Si_3N_4 membrane window was 75 μm × 75 μm × 100 nm (thickness). Based on the burst pressure testing (Fig. 2), the window would break at around 51 bars. Deformation testing was measured up to 47 bars. As shown in Fig. 5, the deformation is defined as the distance between the highest and lowest points in the Z direction (perpendicular to the membrane surface), which is plotted as a function of the applied pressure. The membrane images are taken at different pressures marked by solid circles. It is shown that the deformation increases linearly with the applied pressure when the pressure is low and it tends to saturate when getting closer to the burst pressure. The maximum deformation observed at 47 bars is about 4 μm, which is roughly 5% of the side length of the square Si_3N_4 window.

IV. DEMONSTRATION

To test the performance of the high pressure liquid cell for sXAS, we collected Ca *L*-edge sXAS spectra of 5M $CaCl_2$ aqueous solution at different pressures up to 41 bars, which are shown in Fig. 6(a). For this measurement, the Si_3N_4 window is the same as the one used in the deformation testing (Fig. 5). The Si_3N_4 membrane is in low tensile stress, square shape (75 μm × 75 μm), and 100 nm thick, and the Si frame is 6.35 mm × 6.35 mm × 500 μm. The burst pressure has been tested to be at around 51 bars. Prior to the sXAS experiment, we also tested the mechanical endurance of the Si_3N_4 membrane window, which was repeatedly deformed between 40 and 0 bar for 50 times and remained unbroken. It is the mechanical strength and endurance of the Si_3N_4 window that allows us to further pursue the *in situ* high pressure sXAS experiments. The sXAS measurements are carried out at the undulator beamline, Beamline 8.0.1 of Advanced Light Source, in LBNL.[36] The beam size is focused down to about 50 μm, and the photon flux is about 10^{12} photons per second on the Si_3N_4 window. The sXAS spectra are collected in total fluorescence yield (TFY) using a channeltron electron multiplier and normalized to the beam flux measured by a clean gold mesh. As shown in Fig. 6, the Ca $L_{3,2}$-edge absorption features correspond to the dipole allowed $2p$-$3d$ transitions.[11,37] Although fine features are not well resolved on the spectra due to the low signal-to-noise ratio, it is observed that the relative intensity of the L_3 and L_2 peaks changes with the pressure [Fig. 6(b)]. The Ca $L_{3,2}$-edge absorption edge is sensitive to the local environment of Ca,[38] and it is possible that the observed trend indicates a change in the average number of waters of hydration, which is known to exhibit a marked dependence on temperature.[39] However, the dependence upon pressure is unknown and further study will be required to interpret the spectral change. Nevertheless, this experiment demonstrates the

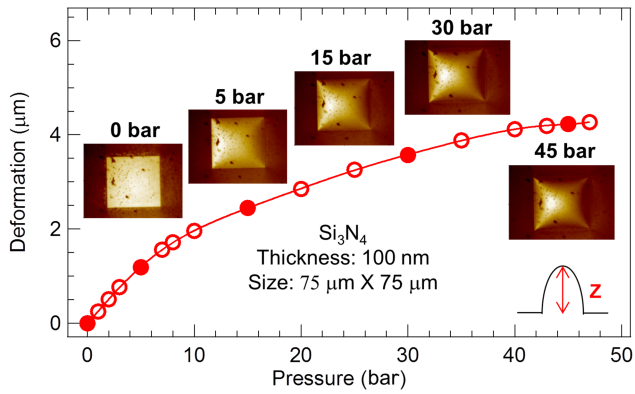

FIG. 5. Deformation of the Si_3N_4 membrane window as a function of applied pressure. The dimension of the Si_3N_4 window is 75 μm × 75 μm × 100 nm (thickness). The deformation is defined as the distance between the highest and lowest points in the Z direction (perpendicular to the membrane surface). The images are taken under different pressures marked by solid circles.

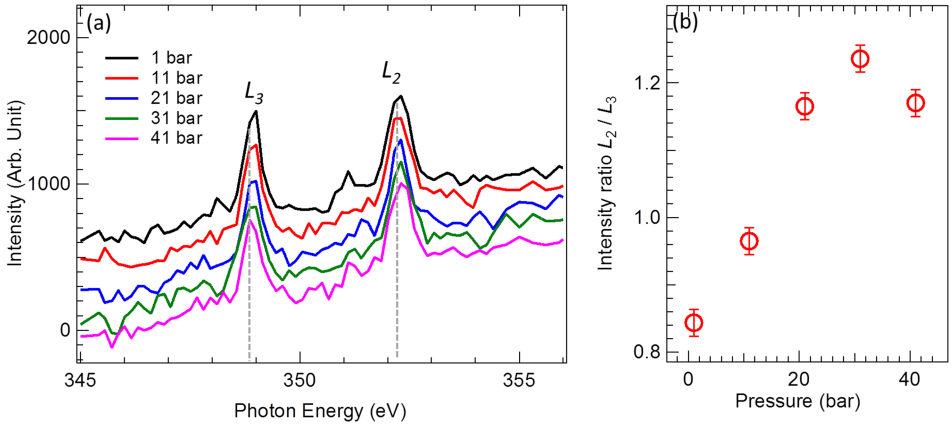

FIG. 6. (a) The Ca *L*-edge x-ray absorption spectra (TFY) of 5M $CaCl_2$ aqueous solution collected at different pressure. All the spectra have been vertically offset and normalized by setting the pre-edge and the L_2 peak at a fixed value. (b) The intensity ratio L_3 and L_2, as a function of the applied pressure.

feasibility and capability of the thin Si_3N_4 membrane window used for the development of the high pressure soft x-ray absorption techniques.

V. CONCLUSION

In conclusion, we have developed the *in situ* high pressure soft x-ray cell. As a demonstration of its performance, the first high pressure sXAS spectra are collected on the Ca *L*-edge of the $CaCl_2$ aqueous solution at different pressures up to 41 bars. The key to this success is the utilization of the superior mechanical strength and endurance of thin Si_3N_4 membrane windows. Comprehensive studies were conducted in order to understand critical factors that affect the hydrostatic strength of the Si_3N_4 membrane window. It is found that the burst pressure of the square Si_3N_4 membrane increases with the decreasing size and is inversely proportional to its side length. The burst pressure also increases proportionally with the membrane thickness. Burst pressures above 60 bars could be achieved for 100 nm-thick square Si_3N_4 windows that are smaller than 65 μm, and particularly the 5 μm Si_3N_4 membrane is predicted to be able to stand the impressive high pressure of 795 bars. However, above a certain pressure, the limiting factor of the burst pressure comes from the breaking of the single crystal Si frame that holds the Si_3N_4 membrane. Similar to the Si_3N_4 membrane, the breaking pressure of the Si frame is related to its thickness. In the current setup that uses two identical O-rings to hold the window and to seal the vacuum, the 500 μm thick Si frame starts to break at around 60 bars. Ways to mitigate the Si frame breaking issue have been discussed and are currently under development. Furthermore, the three-dimensional deformation of the Si_3N_4 membrane is quantified using interferometry. And lastly, we would like to point out that, in addition to the application in the high pressure sXAS cell, the superior mechanical strength and endurance of thin Si_3N_4 membrane windows could also be used in the development of other advanced high pressure characterization tools such as scanning transmission x-ray microscopy (STXM) and transmission electron microscopy (TEM), which requires the separation of the high-pressure liquid/gas under investigation from the vacuum required for x-ray transportation and electron detection. This will provide unprecedented opportunities in many scientific fields for *in situ* and in-operando research of material properties and reactions under high pressure by utilizing the advanced x-ray and electron characterization techniques.

ACKNOWLEDGMENTS

The technical scope of work is supported by the Laboratory Directed Research and Development Program of Lawrence Berkeley National Laboratory under U.S. Department of Energy Contract No. DE-AC02-05CH11231. The Advanced Light Source is supported by the Director, Office of Science, Office of Basic Energy Sciences, of the U.S. Department of Energy under Contract No. DE-AC02-05CH11231. R.Q. is supported by the LDRD program at the Lawrence Berkeley National Laboratory. Y.X. and X.S. are supported by Natural Science Foundation of China (NSFC) (Grant U1432249).

[1]F. de Groot and A. Kotani, *Core Level Spectroscopy of Solids* (CRC Press Taylor & Francis Group, Boca Raton, FL, USA, 2008).
[2]J. G. Tobin, S. W. Yu, R. Qiao, W. L. Yang, C. H. Booth, D. K. Shuh, A. M. Duffin, D. Sokaras, D. Nordlund, and T. C. Weng, Phys. Rev. B **92**(4), 045130 (2015).
[3]X. Liu, J. Liu, R. Qiao, Y. Yu, H. Li, L. Suo, Y.-S. Hu, Y.-D. Chuang, G. Shu, F. Chou, T.-C. Weng, D. Nordlund, D. Sokaras, Y. J. Wang, H. Lin, B. Barbiellini, A. Bansil, X. Song, Z. Liu, S. Yan, G. Liu, S. Qiao, T. J. Richardson, D. Prendergast, Z. Hussain, F. M. F. de Groot, and W. Yang, J. Am. Chem. Soc. **134**(33), 13708–13715 (2012).
[4]P. Olalde-Velasco, J. Jiménez-Mier, J. D. Denlinger, Z. Hussain, and W. L. Yang, Phys. Rev. B **83**(24), 241102 (2011).
[5]R. Qiao, Y. Wang, P. Olalde-Velasco, H. Li, Y.-S. Hu, and W. Yang, J. Power Sources **273**(0), 1120–1126 (2015).
[6]G. Liu, S. Xun, N. Vukmirovic, X. Song, P. Olalde-Velasco, H. Zheng, V. S. Battaglia, L. Wang, and W. Yang, Adv. Mater. **23**(40), 4679–4683 (2011).
[7]X. Shan, D. S. Charles, Y. Lei, R. Qiao, G. Wang, W. Yang, M. Feygenson, D. Su, and X. Teng, Nat. Commun. **7**, 13370 (2016).
[8]R. Qiao, K. Dai, J. Mao, T.-C. Weng, D. Sokaras, D. Nordlund, X. Song, V. S. Battaglia, Z. Hussain, G. Liu, and W. Yang, Nano Energy **16**(0), 186–195 (2015).
[9]R. M. Qiao, L. A. Wray, J. H. Kim, N. P. W. Pieczonka, S. J. Harris, and W. L. Yang, J. Phys. Chem. C **119**(49), 27228–27233 (2015).
[10]E. de Smit, I. Swart, J. F. Creemer, G. H. Hoveling, M. K. Gilles, T. Tyliszczak, P. J. Kooyman, H. W. Zandbergen, C. Morin, B. M. Weckhuysen, and F. M. F. de Groot, Nature **456**(7219), 222–225 (2008).
[11]Y. U. T. Gong, C. E. Killian, I. C. Olson, N. P. Appathurai, A. L. Amasino, M. C. Martin, L. J. Holt, F. H. Wilt, and P. U. P. A. Gilbert, Proc. Natl. Acad. Sci. U. S. A. **109**(16), 6088–6093 (2012).

[12]S. Bernard, B. Horsfield, H. M. Schulz, R. Wirth, A. Schreiber, and N. Sherwood, Mar. Pet. Geol. **31**(1), 70–89 (2012).
[13]M. Nagasaka, H. Yuzawa, and N. Kosugi, J. Electron Spectrosc. Relat. Phenom. **200**, 293–310 (2015).
[14]C. Schwanke, R. Golnak, J. Xiao, and K. M. Lange, Rev. Sci. Instrum. **85**(10), 103120 (2014).
[15]K. Nakanishi, D. Kato, H. Arai, H. Tanida, T. Mori, Y. Orikasa, Y. Uchimoto, T. Ohta, and Z. Ogumi, Rev. Sci. Instrum. **85**(8), 084103 (2014).
[16]M. Nagasaka, H. Yuzawa, T. Horigome, and N. Kosugi, Rev. Sci. Instrum. **85**(10), 104105 (2014).
[17]D. K. Bora, P.-A. Glans, J. Pepper, Y.-S. Liu, C. Du, D. Wang, and J.-H. Guo, Rev. Sci. Instrum. **85**(4), 043106 (2014).
[18]A. Benkert, M. Blum, F. Meyer, R. G. Wilks, W. Yang, M. Bär, F. Reinert, C. Heske, and L. Weinhardt, Rev. Sci. Instrum. **85**(1), 015119 (2014).
[19]J. Guo, J. Electron Spectrosc. Relat. Phenom. **188**, 71–78 (2013).
[20]C. Escudero, P. Jiang, E. Pach, F. Borondics, M. W. West, A. Tuxen, M. Chintapalli, S. Carenco, J. Guo, and M. Salmeron, J. Synchrotron Radiat. **20**(3), 504–508 (2013).
[21]S. Schreck, G. Gavrila, C. Weniger, and P. Wernet, Rev. Sci. Instrum. **82**(10), 103101 (2011).
[22]M. Nagasaka, T. Hatsui, T. Horigome, Y. Hamamura, and N. Kosugi, J. Electron Spectrosc. Relat. Phenom. **177**(2-3), 130–134 (2010).
[23]O. Fuchs, F. Maier, L. Weinhardt, M. Weigand, M. Blum, M. Zharnikov, J. Denlinger, M. Grunze, C. Heske, and E. Umbach, Nucl. Instrum. Methods Phys. Res., Sect. A **585**(3), 172–177 (2008).
[24]B. Winter, Nucl. Instrum. Methods Phys. Res., Sect. A **601**(1), 139–150 (2009).
[25]K. A. Perrine, M. H. C. Van Spyk, A. M. Margarella, B. Winter, M. Faubel, H. Bluhm, and J. C. Hemminger, J. Phys. Chem. C **118**(50), 29378–29388 (2014).
[26]C. Schwanke, L. Xi, and K. M. Lange, J. Synchrotron Radiat. **23**(6), 1390–1394 (2016).
[27]D. Testemale, J. Brugger, W. H. Liu, B. Etschmann, and J. L. Hazemann, Chem. Geol. **264**(1-4), 295–310 (2009).
[28]J. Brugger, A. Pring, F. Reith, C. Ryan, B. Etschmann, W. H. Liu, B. O'Neill, and Y. Ngothai, Radiat. Phys. Chem. **79**(2), 151–161 (2010).
[29]D. L. Gallup, Ore Geol. Rev. **12**(4), 225–236 (1998).
[30]E. J. Beckman, J. Supercrit. Fluids **28**(2-3), 121–191 (2004).
[31]B. Kumar, M. Llorente, J. Froehlich, T. Dang, A. Sathrum, and C. P. Kubiak, Annu. Rev. Phys. Chem. **63**, 541–569 (2012).
[32]I. C. Bourg, L. E. Beckingham, and D. J. DePaolo, Environ. Sci. Technol. **49**(17), 10265–10284 (2015).
[33]D. B. Lee, J. Appl. Phys. **40**(11), 4569–4574 (1969).
[34]J. Pawlak, P. C. Cheng, and D. M. Shinozaki, in *X-Ray Microscopy: Instrumentation and Biological Applications*, edited by P.-C. Cheng and G.-J. Jan (Springer Berlin Heidelberg, Berlin, Heidelberg, 1987), pp. 336–345.
[35]R. Qiao, Q. Li, Z. Zhuo, S. Sallis, O. Fuchs, M. Blum, L. Weinhardt, C. Heske, J. Pepper, M. Jones, A. Brown, A. Spucces, K. Chow, B. Smith, P.-A. Glans, Y. Chen, S. Yan, F. Pan, L. F. J. Piper, J. Denlinger, J. Guo, Z. Hussain, Y.-D. Chuang, and W. Yang, Rev. Sci. Instrum. **88**(3), 033106 (2017).
[36]J. J. Jia, T. A. Callcott, J. Yurkas, A. W. Ellis, F. J. Himpsel, M. G. Samant, J. Stohr, D. L. Ederer, J. A. Carlisle, E. A. Hudson, L. J. Terminello, D. K. Shuh, and R. C. C. Perera, Rev. Sci. Instrum. **66**(2), 1394–1397 (1995).
[37]S. J. Naftel, T. K. Sham, Y. M. Yiu, and B. W. Yates, J. Synchrotron Radiat. **8**(2), 255–257 (2001).
[38]F. J. Himpsel, U. O. Karlsson, A. B. McLean, L. J. Terminello, F. M. F. de Groot, M. Abbate, J. C. Fuggle, J. A. Yarmoff, B. T. Thole, and G. A. Sawatzky, Phys. Rev. B **43**(9), 6899–6907 (1991).
[39]A. A. Zavitsas, J. Phys. Chem. B **109**(43), 20636–20640 (2005).